PCCP

PAPER

View Article Online
View Journal | View Issue

Cite this: *Phys. Chem. Chem. Phys.*, 2024, **26**, 15452

Reproducibility and stability of silane layers in nanoconfined electrochemical systems†

Dominik Duleba, Shekemi Denuga and Robert P. Johnson *

Received 20th March 2024,
Accepted 9th May 2024

DOI: 10.1039/d4cp01181c

rsc.li/pccp

Organosilanes are commonly utilized to attach bioreceptors to oxide surfaces. The deposition of such silane layers is especially challenging in nanoscale or nanoconfined devices, such as in nanopipettes, since rinsing off loosely bound silanes may not be possible due to geometric constrictions and because the thickness of multilayered silanes can cover or block nanoscale features. Furthermore, in electrochemical devices, the silane layers experience additional perturbations, such as electric migration and electroosmotic force. Despite its importance, there appears to be no consensus in the current literature on the optimal methodology for nanopipette silanization, with significant variations in reported conditions. Herein, we systematically investigate the reproducibility and stability of liquid- and vapor-phase deposited silane layers inside nanopipettes. Electrochemical monitoring of the changing internal silanized surface reveals that vapor-deposited APTES generates surface modifications with the highest reproducibility, while vapor-deposited APTMS generates surface modifications of the highest stability over a 24-hour time period. Practical issues of silanizing nanoconfined systems are highlighted, and the importance of carefully chosen silanization conditions to yield stable and reproducible monolayers is emphasized as an underappreciated aspect in the development of novel nanoscale systems.

Introduction

Oxide materials, such as metal and silicon oxides, are widely used in biosensing devices due to their chemical stability, morphological versatility, and physiochemical interfacial properties. Oxide surfaces contain hydroxyl groups that can rapidly form a covalent siloxane bond with silane molecules.[1] As such, bifunctional organosilanes are often used as an intermediary crosslinker to covalently attach bioreceptors to these surfaces to fabricate biosensing devices.[2] Of the many commercially available organosilanes, 3-aminopropyltriethoxysilane (APTES) and 3-aminopropyltrimethoxysilane (APTMS) are most commonly utilized.[3–5]

Ion current rectifying nanopore sensors are oxide-based electrochemical biosensors (when fabricated from quartz or borosilicate glass capillaries) that commonly utilize silane chemistry for bioreceptor attachment. These nanopores, with their nano-scale aperture, are conical-shaped and possess a charged surface due to acidic surface groups. Their diode-like electrical readout is strongly influenced by the magnitude of the surface charge density, where the grafting of an analyte-specific bioreceptor onto the internal nanopore surface allows the capture of various analytes and their subsequent quantification through the extent of surface charge density modulation.[6,7] Organosilanes are typically reported as the crosslinker for immobilizing bioreceptors to internal nanopore surfaces, with procedures adopted from the many numerous examples available for planar silicon oxides. Since the current–voltage curves of ion current rectifying nanopores are highly sensitive to the surface of the nanopore, the deposition of reproducible, homogenous and stable silane layers is essential for optimal biosensor limit-of-detection, stability, and reproducibility.[8]

Unfortunately, grafting reproducible, homogenous, and stable silane layers is not a trivial task as indicated by the extensive literature covering silanization of planar (bulk) surfaces. While the mechanism of the silane layer formation seems straightforward, starting with the hydrolysis of the ethoxy/methoxy groups, followed by condensation to form a siloxane bond, and then phase separation, it is kinetically complex.[9] As such, the characteristics of the layer are heavily influenced by the solvent used, water content, environmental humidity, pH, silane type, silane concentration, reaction time, temperature, and post-silanization treatment.[9–11] In addition to the complex kinetics, there are also various ways in which the organosilane can interact with the surface (Fig. 1).[12] Organosilanes can attach covalently but lie flat on the surface, preventing the reaction of neighbouring surface hydroxyl groups. They can also electrostatically adsorb, or hydrogen bond to the surface, or to other silanes, and polymerize laterally and

School of Chemistry, University College Dublin, Belfield, Dublin 4, Ireland.
E-mail: robert.johnson@ucd.ie

† Electronic supplementary information (ESI) available. See DOI: https://doi.org/10.1039/d4cp01181c

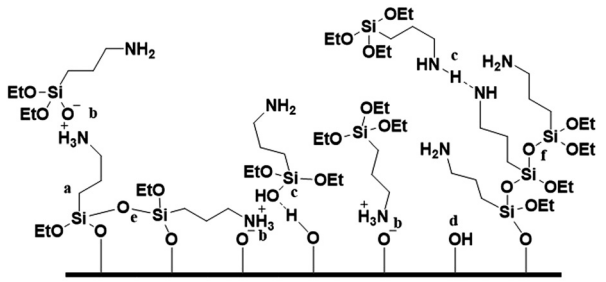

Fig. 1 The types of interactions that may occur between an organosilane and an oxide surface: (a) correctly aligned covalently attachment, (b) electrostatic adsorption to other silanes or to the surface, (c) hydrogen bonding to other silanes or to the surface, (d) unreacted hydroxyl groups, (e) lateral polymerization, and (f) vertical polymerization of silanes.

vertically. This means that silanization can lead to non-homogenous and multilayered silane layers.[13,14] Much of the multilayers, especially weakly adsorbed silanes, are easily washed away by buffer solutions,[2,12,15,16] leading to an alteration of surface coverage and resulting in a nonuniform and inhomogeneous surface.[2,16]

Aside from the weakly bonded layers, even covalently bonded silane molecules can desorb from the surface through hydrolysis of the siloxane bonds.[17] Specifically, amine groups on the organosilane can form a stable five-membered ring intermediate and catalyze the hydrolysis of the siloxane bond.[15] The extent of covalent bonding in silane layers has, however, been questioned, and it has been indicated that APTES layers on the surface are mostly a physically adsorbed network of silanes with sparse anchoring points (<6% of total silane groups).[18] The stability of silane layers is a known issue, and the lack of hydrolytic stabilities of silanes on planar surfaces has been discussed.[10,12,13,15,16]

As the readout of the ion-current rectifying nanopore sensors is strongly dependent on the surface charge, the nature of the silane layer (and the bioreceptors attached to it) is crucial as it will dictate the current–voltage readout of the system (Fig. 2). As such, the aforementioned challenges reported for planar surfaces must be seriously considered. Time-dependent instabilities in the silane layers due to the desorption/rearrangement of weakly/covalently bound silanes can lead to drastic changes in the sensor's readout even in the absence of analyte. Furthermore, attachment of the bioreceptor post-silanization may require multiple hours. If the silane layer is changing during this timeframe, the surface coverage of the bioreceptor may also become non-reproducible and non-homogeneous, resulting in substantially different electrical characteristics between different devices. The already challenging nature of surface silanization may be further complicated by the unique challenges associated with nanopores. For example, electric migration and electroosmotic forces that are act perpendicular to the modified surface could desorb or rearrange weakly adsorbed silanes during electrical measurement. Furthermore, the thickness of silane multilayers (which can range from 0.2–140 nm)[15,19] reported to form under some modification procedures can be comparable to the pore size (~6–250 nm for nanopipettes) and can lead to the alteration of pore radii and/or geometry, with complete or partial blockage.[14] Lastly, in the case of nanopores fabricated by melting and pulling glass capillaries (nanopipettes), rigorous and thorough rinsing of the silanized surface to remove weakly bonded silanes is not possible due to the long conical shape of a nanopipette. Although, the wider part of the nanopipette can be flushed with solvent, convection is restricted in the narrower part of the pipette, and rinsing is essentially limited to displacement by diffusion.

The grafting of a silane monolayer (rather than a multilayer) is desirable for attaining a stable, homogenous and reproducible surface (and hence good device performance).[2,4,13,15] However, the silanization conditions to achieve this for silicon-oxide based biosensors are still unclear,[20,21] and even less so for nanoconfined devices, such as ion-current rectifying nanopore sensors. The reported silanization conditions for nanopipettes vary substantially (Table 1), with studies, (including in our own laboratory) often applying a trial-and-error approach towards obtaining a satisfactory silane layer, or utilizing parameters based on planar surface silanization results.[4,8] To the best of our knowledge, the stability and reproducibility of silanization has not previously been systematically investigated for nanopipette systems. Herein, we investigate the reproducibility and stability of silane layers in nanopipettes where silanization is carried out under various modification conditions and with different silanes. We show the stability and reproducibility of APTES and APTMS silanization carried out in ethanol, as well as APTES and APTMS silanization carried out in the vapor-phase, with the aim of identify an improved procedure, and highlighting potential issues with silanization techniques.

Experimental procedures

Materials and reagents

Potassium chloride (KCl) 99+% and ethanol were obtained from Fisher Scientific, 3-aminopropyltriethoxysilane (APTES) from Tokyo Chemical Industry and 3-aminopropyltrimethoxysilane (APTMS) from Fluorochem. Ag/AgCl electrodes were prepared in-house using 0.25 mm silver wires obtained from Fisher Scientific. All solutions were prepared using ACS reagent water from Sigma-Aldrich. Filamented glass capillaries with 1 mm outer diameter and 0.7 mm internal diameter were obtained from WPI. Fused quartz wafers were obtained from Thermo Scientific.

Nanopipette fabrication

A P-2000 laser pipette puller from Sutter was used to prepare conical quartz nanopipettes with pore radii of 60 nm (line 1: H700 F4 V20 D170 P0, line 2: H680 F4 V50 D170 P200). Capillaries were cleaned with isopropyl alcohol prior to pulling. Nanopipettes with pulling times outside of the expected 4.6 ± 0.2 s were discarded.

Silanization procedures

The surface is not pre-treated before silanization in these experiments.

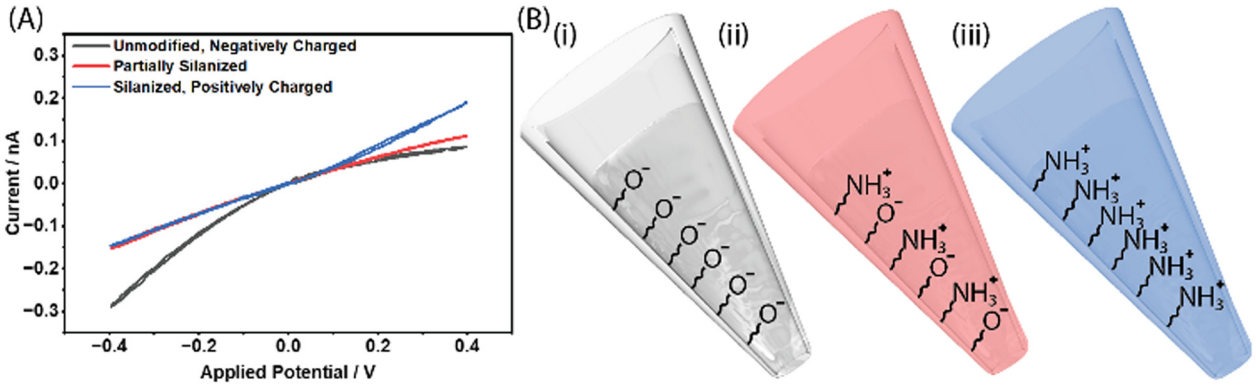

Fig. 2 (A) The diode-like (non-ohmic) current–voltage curves of (i) a highly negatively charged nanopipette, (ii) a slightly negatively charged nanopipette (partial coverage with a low surface density of grafted silane molecules) and (iii) a highly positively charged nanopipette (positive charge arising from a high surface density of grafted silane molecules). The non-ohmic response arises where the electric double layers of the nanopore interact with the ionic flux through the aperture and impose an ionic permselectivity.[22,23] This leads to an ionic enrichment at one applied potential that results in a high conductance ON-state, while the opposite potential leads to an ionic depletion, resulting in a low conductance OFF-state.[24–29] The potentials at which the ON- and OFF-states are observed depend on whether the nanopore is cation or anion permselective, which in turn depends on the surface charge of the nanopore.

Table 1 Silanization procedures reported for nanopipettes

Pre-treatment	Silane	Concentration	Solvent	Reaction	Post-treatment	
Piranha	APTES	5%	Ethanol	2 h	120 °C for 1 h	30
Piranha	APTES	5%	Ethanol	1 h	120 °C for 1 h	31
	APTES	1%	Ethanol	2 h	110 °C for 1 h (vacuum)	32
	APTES	1%	Ethanol		120 °C for 2 h	33
Piranha (0.5 h)	APTES	0–1.1%,	Ethanol	0–4 h	110 °C for 0.5 h	34
	APTMS	1%	Acetone	4 °C for 12 h	120 °C for 1 h	35
Boiling H_2O_2 (0.5 h)	APTMS	11%	Acetone	Overnight	120 °C for 1 h	36
	APTMS	Vapour-phase	Vapour-phase	40 °C for 1 h		37 and 38
	TESPG	2.5%	Ethanol	Overnight	N_2 dry	39
Piranha (24 h)	DHITES	0.74 mM	Ethanol	Overnight		40
	DHITES	17%	Ethanol	Overnight		41
Piranha (24 h)	ATMS	1 mM	Ethanol	Overnight		42
Piranha (2 h)	TESP-SA	1%	Isopropanol	1 h	60 °C for 1.5 h (vacuum)	43
Piranha	TESBA	5%	Ethanol, acetate buffer (pH 4.7)	20 h		44
	MPTES	0.01%	Ethanol	15 min	60 °C for 2–3 h	45
Boiling H_2O_2 (20 min)	MPTMS	10%	Ethanol	4 h	120 °C	46

Liquid-phase. 1% silane (APTES or APTMS) in ethanol is backfilled into the nanopipettes using a microsyringe. The tips of the nanopipettes are dipped into the same silane solution, and the nanopipettes are covered to prevent the evaporation of ethanol and a change in the silane concentration. After a 1-hour reaction time, the silane solution is removed with the microsyringe, and the exterior and interior are flushed with copious amounts of ethanol. The pipettes are dried at 70° C for 1 hour, then baked at 110° C for 30 minutes.

Vapor-phase. 200 μL of silane (APTES or APTMS) is placed in the bottom of a desiccator, with the nanopipettes placed on the desiccator plate with Blu Tack. The desiccator is put under vacuum and placed in a 40° C water bath for 1 hour. The nanopipettes are then transferred to the oven for a 1-hour bake at 120° C. For triple silanization, the silane deposition and baking steps are sequentially repeated.

Electrochemical measurements

For electrochemical measurements, the nanopipettes were backfilled with 1 mM KCl. The current–voltage curves were measured with a two-electrode (Ag/AgCl and Ag/AgCl) setup using a Biologic SP-200 potentiostat fitted with the ultra-low-current (ULC) option. A scan rate of 0.05 V s^{-1} is used to scan within the −0.4 V to +0.4 V potential window. A 5 Hz filter bandwidth is used to reduce noise. Over the 24-hour desorption period, the nanopipettes were kept wet and left in the measurement solution. Both the external solution and the nanopipettes were sealed to prevent evaporation. The cell was left undisturbed within the Faraday cage for the entire period.

Contact angle measurements

Quartz wafers were cleaned with acidic Piranha solution (3 : 1 c. sulfuric acid: 30% hydrogen peroxide) and ultrasonicated in acetone prior to silanization. The contact angles of silanized quartz wafers were measured, and then they were placed in 1 mM KCl for 24 hours, rinsed with water, and oven-dried. The contact angles were then remeasured. Contact angles were measured with a KRÜSS DSA25 fitted with the CM4210 optics module. On each wafer, a total of seven 2 μL (estimated volume from diameter: 2.23 ± 0.02 μL) droplets were deposited at a rate

of 1 μL s^{-1}. Triple-distilled water was used. Droplet fitting was done with an automatic baseline to minimize human bias.

Scanning transmission electron microscopy

STEM images were taken with a Zeiss Sigma300 FEG SEM with a STEM detector and a 10 kV acceleration.

Results and discussion

The stability and reproducibility of the two most commonly used silanes in nanopipette modification, APTES and APTMS, are investigated by grafting them to the internal walls of 60 nm radius quartz nanopipettes (Fig. S1, ESI†) using both liquid- and vapor-phase approaches. The unmodified bare nanopipette surfaces are covered with predominantly Si–O^- groups at pH 7.[47] A negatively charged surface generates a negatively rectifying current–voltage response, with the ON-state at the negative applied potential (Fig. 2). Grafting of APTES/APTMS *via* the condensation reaction of the triethyoxy/trimethoxy groups with the surface silanol groups results in an amine-terminated surface, where the dissociation constant of the $-NH_2$ group is *ca.* 7.4.[48] This will result in an overall positively charged surface at pH 7, swapping the nanopipette's ON-state to the positive applied potential, and confirming the success of silanization (Fig. 2). The continuous desorption of silane molecules from the surface should then remove positive charges from the surface, gradually shifting the current–voltage curves back to their original state, where the ON-state is observed at the negative applied potential due to the negative surface charge densities.

Silanized nanopipette filling and blockage/De-wetting

Silane grafting, especially in the liquid-phase, is fraught with practical problems. Liquid-phase silane layers are heterogenous and possess high surface roughness,[10,13–15,20] due to silane clusters at areas of high surface roughness where amine moieties do not fully orient outwards, exposing their hydrophobic alkyl chains.[11,20] This results in the variation of the surface hydrophobicity along the neck of the nanopipette which disrupts the advance of the meniscus during nanopipette backfilling (where the solution inside the nanopipette is drawn into the nanoscale tip *via* capillary forces). This results in significant challenges in filling the nanopipettes, leading to a high attrition rate where the neck of the pipette couldn't be completely filled, and an electrical circuit could not be established. Vapor-phase silane deposition produces smoother and less hydrophobic surfaces as the lower water presence is detrimental to copolymerization,[14,15,20] and the amine moieties tend to consistently orient outwards. Contact angle measurements on planar quartz wafers confirm higher contact angles for liquid-phase deposited silanes than for vapor-phase deposition (Table S1, ESI†). As a result of the smoother and less hydrophobic surface, nanopipette filling for vapor-deposited silanes is very reliable, with an attrition rate close to 0%.

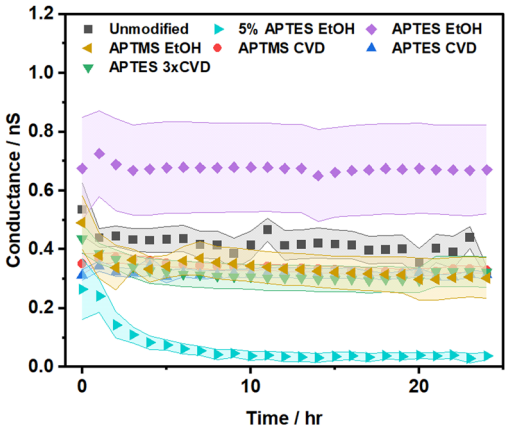

Fig. 3 The conductance of nanopipettes over 24 hours, illustrating that while 5% APTES it EtOH results in a blocked pore, the other modifications remain open and conductive. Each data point is the average of at least 5 nanopipette measurements, with the shaded area indicating ± standard error. The higher conductance of the nanopipettes silanized in 1% APTES in EtOH can be attributed to the formation of an extensive cationic polymer layer on the nanopore surface.[50] Sample cyclic voltammograms for blocked and unblocked nanopipettes are provided in Fig. S2 (ESI†).

Even the nanopipettes successfully filled after liquid-phase silanization can provide unsatisfactory results. Liquid-phase silanization with more concentrated silanes (5% APTES in EtOH) leads to the loss of conductance, and subsequent breakage of the electric circuit after a few hours (Fig. 3). This loss of conductance could be the result of the physical blockage and/or spontaneous de-wetting of the nanopipette mouth as desorbed polymer aggregates coagulate in the pore mouth. Pore blockage has been previously reported for meso-porous materials.[14,49] As such it becomes apparent, that setting up the silanization conditions to minimize polymerization is important, as it will minimize the extent of polymer aggregation on the surface and prevent the desorbed aggregates from coagulating at the tip. This can be achieved by decreasing the silane concentration (although such blockage/de-wetting can still happen with a lower frequency) or by changing to a vapor-phase method. Fig. 3 shows that vapor-deposited silane layers, and lower concentrations (1%) of liquid-phase silanization lead to a more stable electrical circuit where the conductance is stable.

Reproducibility and extent of silanization

The ability to reproducibly graft silane on the surface of the nanopipette is important for ensuring device to device comparability, particularly where the silane layer is the pre-cursor to the grafting of a biorecognition element that will give a quantitative response to an analyte of interest. A good descriptor for evaluating the outcome of the modification and for monitoring the continuously changing surface as the silane is desorbing, is the logarithmic rectification ratio (logRR):

$$\log\mathrm{RR} = \log\left|\frac{I(-E)}{I(+E)}\right|$$

where $I(-E)$ is the current at a negative applied potential and $I(+E)$ is the current at the same positive applied potential. In this work, the currents at +0.4 V and −0.4 V are used.

The rectification ratio describes the extent of the diode-like behavior of the system. If the ON-state is at the negative applied potential (as is the case for net negative surface charge densities), the current at the negative applied potential will be greater than that at the positive applied potential, and the logarithmic rectification ratio will be greater than 0. On the other hand, for net positive surface charge densities where the ON-state is at the positive applied potential, the logarithmic rectification ratio will be less than 0. As such, the rectification ratio describes the sign and magnitude of the surface charge density, which is related to the extent and distribution of the silane layer. The rectification ratio is a composite parameter that does not provide direct information about the resistivity at a single applied potential, but describes the surface charge of the nanopipette qualitatively. We use the logarithmic rectification ratio instead of the more commonly utilized rectification ratio, $|I(-V)/I(+V)|$, as the latter is an asymmetric metric, *i.e.*, nanopipettes with their ON-state at the negative potentials can take on values from $1 \rightarrow \infty$, while nanopipettes with their ON-state at the positive potentials have a range of $0 \rightarrow 1$, as such the distributions of multiple measurements of negatively charged and positively charged nanopipettes would not be directly comparable (Fig. S3, ESI†). Using the logarithmic value centers the metric on zero and makes the metric symmetric above and below unity, allowing for better comparison of values.

Fig. 4 shows the distribution of the logarithmic rectification ratio for nanopipettes modified with different silanes and with different silanization methods. Compared to the unmodified nanopipettes, the rectification ratio of the silane-functionalized nanopipettes is decreased, indicating successful silanization. The mean logRR of the liquid-phase silanization is lower than that of vapor-phase, which is consistent with liquid-phase silanization grafting multilayers of polymerized silanes that add a larger positive surface charge density to the surface than the monolayers grafted at vapor-phase. The rectification ratio of nanopipettes that underwent multiple rounds of vapor-phase deposition is lower than those that underwent a single round, indicating that gaps in the surface coverage remained and were filled.

The standard deviation of the logarithmic rectification ratio can be used to evaluate the reproducibility of silanization. Fig. 4 shows that the distribution of logRR for liquid-phase deposited silanes is wider than those of vapor-phase. This is in line with previous works at bulk surfaces that have noted a substantial issue with the reproducibility of even anhydrous liquid-phase silane layers due to self-polymerization in the presence of trace water.[20] Vapor-phase deposited APTES has the highest reproducibility, with standard deviations only marginally greater than that of the unmodified nanopipettes. This indicates that the variance that originates from APTES vapor-phase deposition is small compared to the variance associated with the nanopipette's geometric variability (which is the main source of

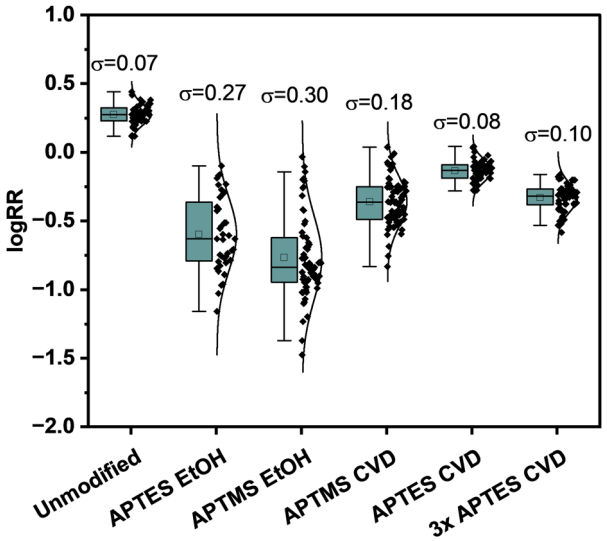

Fig. 4 Box-and-whisker plots of the initial logarithmic rectification ratios recorded (before nanopipettes are monitored for 24 hours). The standard deviation of each method is also given in the figure.

variance for the unmodified nanopipettes). The higher reproducibility of vapor-phase deposition can be attributed to environmental factors, such as temperature, silane purity, and ambient humidity, having a decreased influence compared to liquid-phase deposition.[51] Furthermore, vapor-phase deposition produces more homogenous surfaces as non-dimerized and non-oligomerized silane precursors have a higher vapor pressure, as such they are the dominant species to react with the surface.[11,14,15,51] These more homogenous monolayers are expected to have lower structural variations than the polymerized multilayers produced by liquid-phase approaches. Lastly, experimental variations are greatly reduced with vapor-phase deposition, as removal of solvent, rinsing, and transferring between vessels is less time consuming. Consequently, the throughput of the vapor-phase method is very high. The batch size of the vapor-phase approach was 60 nanopipettes, but scaling the batch size further is simply a matter of the desiccator vessel size. This is a considerable practical advantage compared to the tedious liquid-phase approach.[52]

Stability of silane layers

Silane-functionalized planar surfaces (with no electrochemical perturbations) have been widely reported to have poor hydrolytic stability.[15] Additionally, our contact angle measurements also show that for all silane deposition methods reported in this work, the contact angles of silanized planar quartz wafers decrease upon exposure to an electrolyte solution for 24 hours, indicating the desorption of the silane layers (Table S1, ESI†). Silane layers on the planar quartz surface do not experience the electric fields (and hence the electric migration and electroosmotic forces) and local concentration polarization that the nanopipettes experience during the electrochemical measurement. This is important to consider, as in nanopipettes, the electric migration and electroosmotic forces are parallel to the

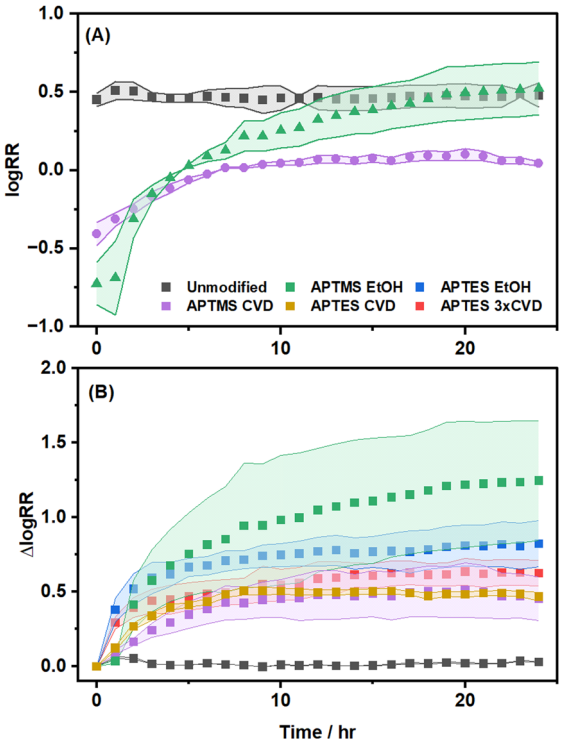

Fig. 5 (A) Logarithmic rectification ratios over 24 hours of the most and least stable silanization methods, and (B) change in the logarithmic rectification ratio over 24 hours shown for all silanization methods. Each curve is the average of at least 5 nanopipette measurements. Sample curves of both the logRR and the ΔlogRR for individual nanopipettes and for comparing each modification to the unmodified nanopipette are provided in Fig. S5–S8 (ESI†).

silanized surface, as such in addition the silane normally desorbing, weakly bound silanes could also be dragged along the nanopipette surface. The influence of electroosmotic flow is expected to be concentration dependent as the magnitude of surface charge density itself is concentration dependent,[47] however, herein only 1 mM concentration is explored. The electroosmotic force acting parallel to the surface implies that not only do the silane layers desorb, changing the surface coverage and charge density, but they may also rearrange along the nanopore, altering the distributions of the silane layer and surface charge. Nanopipettes are highly sensitive to such changes in surface charge distribution, especially near the tip region.[53–55] The rectification ratio was used to monitor the combined effect of these changes as a function of time (Fig. 5). As shown in Fig. 5, the unmodified nanopipettes are stable over 24 hours, meaning that the changes observed for the silanized nanopipettes can be attributed to the silane layers. The logarithmic rectification ratios of all silanized nanopipettes increase over time (approaching the logRR of the unmodified nanopipettes). Although all grafted silane layers change over the course of 24 hours, the vapor-phase deposited silanes show better stability, with the best stabilities observed for vapor-deposited APTMS.

The improved stability of vapor-phase modified nanopipettes, compared to those prepared by liquid-phase silanization can be attributed to the formation of denser and more ordered monolayers. Vapor-phase silanization has been shown to deposit a homogenous monolayer in the bulk.[15,51] This is partly because of a difference in the physisorption mechanism. During vapor-phase silanization, the physisorption of monomer silanes (due to their higher vapor pressure) is predominant. The adsorbed monomers can form a higher density layer on the substrate, allowing for the formation of a higher density of anchoring points during bond formation. In liquid-phase silanization, monomers adsorb simultaneously with polymers, with large polymer aggregates blocking the surface, preventing the adsorption of monomers, resulting in a lower coverage of molecules capable of forming an anchoring point with the substrate.[56] The density of anchoring points has been recently highlighted as an important consideration by Millot *et al.* who argued that liquid-phase silane layers may possess only sparse anchoring points (<6% of total silane groups).[18] The higher density of anchoring points would necessitate the hydrolysis of more siloxane bonds before covalently attached silane molecules can be lost. Although the preferred adsorption of monomer silanes during vapor-phase silanization would result in a more ordered silane layer, differences in the attachment mechanisms could also play a role. Due to the lack of solution-phase water in vapor-phase silanization, the siloxane bond is formed *via* condensation with surface adsorbed trace water, the amount of which was shown to influence the resulting silane coverage,[56] or in the absence of surface adsorbed water, *via* direct nucleophilic attack during the baking process.[16] This attachment mechanism may allow for a more ordered silane layer compared to liquid-phase silanization. The more ordered and more dense vapor-phase deposited silane layer would be expected to have improved stability as the anchoring silicon center is sterically protected by the aliphatic tails from hydrolytic and self-catalytic cleavage.

Conclusions

To conclude, silane stability and reproducibility should be seriously considered when designing a nanopore sensor. We have highlighted the practical problems of nanopore blockage/dewetting and showed that vapor-phase deposition leads to the most reproducible current–voltage readouts of silanized nanopipettes. The monitoring of contact angle measurement and current–voltage curves over 24 hours highlighted the changing nanopore surface and has identified the vapor-phase method as the preferred method to obtain a stable surface. We have also noted the considerably higher throughput of vapor-phase deposition and made a case that it should be the preferred silanization method for the nanopore community. However, distinguishing the underlying mechanism of silane layer desorption in nanoconfined systems requires further investigation. Where, for example, establishing the concentration and pH-dependence of the stability, as well as using silanes with different chain lengths and functionalities, and/or capping-off the amine with a protecting group to distinguish the influence

of self-catalyzed hydrolysis, may provide further insights into the underlying surface chemistry.

Author contributions

Dominik Duleba – conceptualization, formal analysis, investigation, methodology, visualization, writing (original draft), writing (review & editing). Shekemi Denuga – investigation, writing (review & editing). Robert P. Johnson – conceptualization, supervision, project administration, writing (review & editing).

Conflicts of interest

There are no conflicts to declare.

Acknowledgements

We acknowledge funding from Science Foundation Ireland under the Frontiers for the Future Programme (Project No. 20/FFP-P/8728). DD acknowledges Postgraduate scholarship funding from the Irish Research Council (Project No. GOIPG/2022/1648) and SD acknowledges funding from the National University of Ireland for a Travelling Doctoral Scholarship.

References

1 G. L. Witucki, A Silane Primer: Chemistry and Applications of Alkoxy Silanes, *J. Coat. Technol.*, 1993, **65**, 57–60.
2 N. S. K. Gunda, M. Singh, L. Norman, K. Kaur and S. K. Mitra, Optimization and Characterization of Biomolecule Immobilization on Silicon Substrates Using (3-Aminopropyl)Triethoxysilane (APTES) and Glutaraldehyde Linker, *Appl. Surf. Sci.*, 2014, **305**, 522–530, DOI: 10.1016/j.apsusc.2014.03.130.
3 M. Hijazi, V. Stambouli, M. Rieu, V. Barnier, G. Tournier, T. Demes, J.-P. Viricelle and C. Pijolat, Synthesis and Characterization of Tin Dioxide Thick Film Modified by APTES in Vapor and Liquid Phases, *J. Mater. Sci.*, 2018, **53**(1), 727–738, DOI: 10.1007/s10853-017-1541-4.
4 M. Antoniou, D. Tsounidi, P. S. Petrou, K. G. Beltsios and S. E. Kakabakos, Functionalization of Silicon Dioxide and Silicon Nitride Surfaces with Aminosilanes for Optical Biosensing Applications, *Med. Devices Sens.*, 2020, **3**(5), e10072, DOI: 10.1002/mds3.10072.
5 A. Miranda, L. Martínez and P. A. A. De Beule, Facile Synthesis of an Aminopropylsilane Layer on Si/SiO_2 Substrates Using Ethanol as APTES Solvent, *MethodsX*, 2020, **7**, 100931, DOI: 10.1016/j.mex.2020.100931.
6 D. Duleba and R. P. Johnson, Sensing with Ion Current Rectifying Solid-State Nanopores, *Curr. Opin. Electrochem.*, 2022, **34**, 100989.
7 S. Zhang, W. Chen, L. Song, X. Wang, W. Sun, P. Song, G. Ashraf, B. Liu and Y.-D. Zhao, Recent Advances in Ionic Current Rectification Based Nanopore Sensing: A Mini-Review, *Sens. Actuators Rep.*, 2021, 100042.
8 M. Sypabekova, A. Hagemann, D. Rho and S. Kim, Review: 3-Aminopropyltriethoxysilane (APTES) Deposition Methods on Oxide Surfaces in Solution and Vapor Phases for Biosensing Applications, *Biosensors*, 2022, **13**(1), 36, DOI: 10.3390/bios13010036.
9 A. A. Issa and A. S. Luyt, Kinetics of Alkoxysilanes and Organoalkoxysilanes Polymerization: A Review, *Polymers*, 2019, **11**(3), 537, DOI: 10.3390/polym11030537.
10 E. T. Vandenberg, L. Bertilsson, B. Liedberg, K. Uvdal, R. Erlandsson, H. Elwing and I. Lundström, Structure of 3-Aminopropyl Triethoxy Silane on Silicon Oxide, *J. Colloid Interface Sci.*, 1991, **147**(1), 103–118, DOI: 10.1016/0021-9797(91)90139-Y.
11 X. Song, J. Zhai, Y. Wang and L. Jiang, Self-Assembly of Amino-Functionalized Monolayers on Silicon Surfaces and Preparation of Superhydrophobic Surfaces Based on Alkanoic Acid Dual Layers and Surface Roughening, *J. Colloid Interface Sci.*, 2006, **298**(1), 267–273, DOI: 10.1016/j.jcis.2005.11.048.
12 E. Asenath Smith and W. Chen, How To Prevent the Loss of Surface Functionality Derived from Aminosilanes, *Langmuir*, 2008, **24**(21), 12405–12409, DOI: 10.1021/la802234x.
13 A. R. Yadav, R. Sriram, J. A. Carter and B. L. Miller, Comparative Study of Solution Phase and Vapor Phase Deposition of Aminosilanes on Silicon Dioxide Surfaces, *Mater. Sci. Eng., C*, 2014, **35**, 283–290, DOI: 10.1016/j.msec.2013.11.017.
14 V. G. P. Sripathi, B. L. Mojet, A. Nijmeijer and N. E. Benes, Vapor Phase *versus* Liquid Phase Grafting of Meso-Porous Alumina, *Microporous Mesoporous Mater.*, 2013, **172**, 1–6, DOI: 10.1016/j.micromeso.2013.01.013.
15 M. Zhu, M. Z. Lerum and W. Chen, How to Prepare Reproducible, Homogeneous, and Hydrolytically Stable Aminosilane-Derived Layers on Silica, *Langmuir*, 2012, **28**, 416–423.
16 N. Aissaoui, L. Bergaoui, J. Landoulsi, J.-F. Lambert and S. Boujday, Silane Layers on Silicon Surfaces: Mechanism of Interaction, Stability, and Influence on Protein Adsorption, *Langmuir*, 2012, **28**(1), 656–665, DOI: 10.1021/la2036778.
17 C. M. Dekeyser, C. C. Buron, K. Mc Evoy, C. C. Dupont-Gillain, J. Marchand-Brynaert, A. M. Jonas and P. G. Rouxhet, Oligo(Ethylene Glycol) Monolayers by Silanization of Silicon Wafers: Real Nature and Stability, *J. Colloid Interface Sci.*, 2008, **324**(1), 118–126, DOI: 10.1016/j.jcis.2008.05.002.
18 Y. Millot, A. Hervier, J. Ayari, N. Hmili, J. Blanchard and S. Boujday, Revisiting Alkoxysilane Assembly on Silica Surfaces: Grafting *versus* Homo-Condensation in Solution, *J. Am. Chem. Soc.*, 2023, **145**(12), 6671–6681, DOI: 10.1021/jacs.2c11390.
19 Y. Han, D. Mayer, A. Offenhäusser and S. Ingebrandt, Surface Activation of Thin Silicon Oxides by Wet Cleaning and Silanization, *Thin Solid Films*, 2006, **510**(1), 175–180, DOI: 10.1016/j.tsf.2005.11.048.
20 S. Fiorilli, P. Rivolo, E. Descrovi, C. Ricciardi, L. Pasquardini, L. Lunelli, L. Vanzetti, C. Pederzolli, B. Onida and E. Garrone, Vapor-Phase Self-Assembled Monolayers of Aminosilane on Plasma-Activated Silicon Substrates, *J. Colloid Interface Sci.*, 2008, **321**(1), 235–241, DOI: 10.1016/j.jcis.2007.12.041.

21 C. M. Halliwell and A. E. G. Cass, A Factorial Analysis of Silanization Conditions for the Immobilization of Oligonucleotides on Glass Surfaces, *Anal. Chem.*, 2001, **73**(11), 2476–2483, DOI: **10.1021/ac0010633**.

22 Z. Siwy, E. Heins, C. C. Harrell, P. Kohli and C. R. Martin, Conical-Nanotube Ion-Current Rectifiers: The Role of Surface Charge, *J. Am. Chem. Soc.*, 2004, **126**, 10850–10851.

23 Z. Siwy and A. Fuliński, A Nanodevice for Rectification and Pumping Ions, *Am. J. Phys.*, 2004, **72**, 567–574.

24 D. Woermann, Analysis of Non-Ohmic Electrical Current–Voltage Characteristic of Membranes Carrying a Single Track-Etched Conical Pore, *Nucl. Instrum. Methods Phys. Res., Sect. B*, 2002, **194**, 458–462.

25 D. Woermann, Electrochemical Transport Properties of a Cone-Shaped Nanopore: High and Low Electrical Conductivity States Depending on the Sign of an Applied Electrical Potential Difference, *Phys. Chem. Chem. Phys.*, 2003, **5**, 1853–1858.

26 D. Woermann, Electrochemical Transport Properties of a Cone-Shaped Nanopore: Revisited, *Phys. Chem. Chem. Phys.*, 2004, **6**, 3130–3132.

27 J. Cervera, B. Schiedt and P. Ramirez, A Poisson/Nernst-Planck Model for Ionic Transport through Synthetic Conical Nanopores, *Europhys. Lett.*, 2005, **71**, 35–41.

28 J. Cervera, B. Schiedt, R. Neumann, S. Mafé and P. Ramírez, Ionic Conduction, Rectification, and Selectivity in Single Conical Nanopores, *J. Chem. Phys.*, 2006, **124**, 104706.

29 D. Duleba, P. Dutta, S. Denuga and R. P. Johnson, Effect of Electrolyte Concentration and Pore Size on Ion Current Rectification Inversion, *ACS Meas. Sci. Au*, 2022, **2**, 271–277.

30 S. Chen, H. Chen, J. Zhang, H. Dong, K. Zhan and Y. Tang, A Glass Nanopore Ionic Sensor for Surface Charge Analysis, *RSC Adv.*, 2020, **10**, 21615–21620.

31 W. Ma, W. Xie, R. Tian, X. Zeng, L. Liang, C. Hou, D. Huo and D. Wang, An Ultrasensitive Aptasensor of SARS-CoV-2 N Protein Based on Ion Current Rectification with Nanopipettes, *Sens. Actuators, B*, 2023, **377**, 133075, DOI: **10.1016/j.snb.2022.133075**.

32 S. Zhang, H. Chai, K. Cheng, L. Song, W. Chen, L. Yu, Z. Lu, B. Liu and Y.-D. Zhao, Ultrasensitive and Regenerable Nanopore Sensing Based on Target Induced Aptamer Dissociation, *Biosens. Bioelectron.*, 2020, **152**, 112011.

33 F.-F. Liu, X.-P. Zhao, X.-W. Liao, W.-Y. Liu, Y.-M. Chen and C. Wang, Ultrasensitive and Label-Free Detection of Cell Surface Glycan Using Nanochannel-Ionchannel Hybrid Coupled with Electrochemical Detector, *Anal. Chem.*, 2020, **92**, 5509–5516.

34 G.-C. Liu, W. Chen, M.-J. Gao, L.-B. Song, X.-Y. Hu and Y.-D. Zhao, Ion-Current-Rectification-Based Customizable pH Response in Glass Nanopipettes *via* Silanization, *Electrochem. Commun.*, 2018, **93**, 95–99.

35 X.-P. Zhao, F.-F. Liu, W.-C. Hu, M. R. Younis, C. Wang and X.-H. Xia, Biomimetic Nanochannel-Ionchannel Hybrid for Ultrasensitive and Label-Free Detection of microRNA in Cells, *Anal. Chem.*, 2019, **91**, 3582–3589.

36 X.-P. Zhao, Y. Zhou, Q.-W. Zhang, D.-R. Yang, C. Wang and X.-H. Xia, Nanochannel–Ion Channel Hybrid Device for Ultrasensitive Monitoring of Biomolecular Recognition Events, *Anal. Chem.*, 2018, **91**, 1185–1193.

37 N. Nakatsuka, A. Faillétaz, D. Eggemann, C. Forró, J. Vörös and D. Momotenko, Aptamer Conformational Change Enables Serotonin Biosensing with Nanopipettes, *Anal. Chem.*, 2021, **93**, 4033–4041.

38 N. Nakatsuka, K. J. Heard, A. Faillétaz, D. Momotenko, J. Vörös, F. H. Gage and K. C. Vadodaria, Sensing Serotonin Secreted from Human Serotonergic Neurons Using Aptamer-Modified Nanopipettes, *Mol. Psychiatry*, 2021, **26**(7), 2753–2763, DOI: **10.1038/s41380-021-01066-5**.

39 V. Cayón, G. Laucirica, Y. T. Terrones, M. L. Cortez, G. Pérez-Mitta, J. Shen, C. Hess, M. E. Toimil-Molares, C. Trautmann and W. A. Marmisollé, Borate-Driven Ionic Rectifiers Based on Sugar-Bearing Single Nanochannels, *Nanoscale*, 2021, **13**, 11232–11241.

40 X. Liu, Q. Zeng, C. Liu, J. Yang and L. Wang, Experimental and Finite Element Method Studies for Femtomolar Cobalt Ion Detection Using a DHI Modified Nanochannel, *Analyst*, 2019, **144**, 6118–6127.

41 N. Sa, Y. Fu and L. A. Baker, Reversible Cobalt Ion Binding to Imidazole-Modified Nanopipettes, *Anal. Chem.*, 2010, **82**(24), 9963–9966, DOI: **10.1021/ac102619j**.

42 X. Liu, C. Liu, J. Yang, R. Zhang, Q. Zeng and L. Wang, Detection and FEM Studies of Dichromate ($Cr_2O_7^{2-}$) by Allyltriethoxysilane Modified Nanochannel, *J. Electroanal. Chem.*, 2020, **858**, 113818.

43 D. Wang, G. Qi, Y. Zhou, H. Li, Y. Zhang, C. Xu, P. Hu and Y. Jin, Glucose Level Determination in Single Cells in Their Satiety and Starvation States Using an Enzymatic Functional Glass Nanopore, *Chem. Commun.*, 2020, **56**, 5393–5396.

44 Y. Fu, H. Tokuhisa and L. A. Baker, Nanopore DNA Sensors Based on Dendrimer-Modified Nanopipettes, *Chem. Commun.*, 2009, 4877–4879.

45 Q. Shen, P.-L. Zhou, B.-T. Huang, J. Zhou, H.-L. Liu, S. A. Ahmed, X.-L. Ding, J. Li, Y.-M. Zhai and K. Wang, Mass Transport through a Sub-10 Nm Single Gold Nanopore: SERS and Ionic Current Measurement, *J. Electroanal. Chem.*, 2021, **894**, 115373.

46 S. Guan, J. Yue, W. Sun, W. Xu, C. Liang and S. Xu, Ultrasensitive Detection of Trypsin in Serum *via* Nanochannel Device, *Anal. Bioanal. Chem.*, 2021, **413**, 4939–4945.

47 D. Duleba and R. P. Johnson, Proton Enrichment and Surface Charge Dynamics in pH-Responsive Nanopipettes, *Electrochim. Acta*, 2024, **479**, 143838, DOI: **10.1016/j.electacta.2024.143838**.

48 H. Zhang, H.-X. He, J. Wang, T. Mu and Z.-F. Liu, Force Titration of Amino Group-Terminated Self-Assembled Monolayers Using Chemical Force Microscopy, *Appl. Phys. A: Mater. Sci. Process.*, 1998, **66**(1), S269–S271, DOI: **10.1007/s003390051143**.

49 F.-Y. Chang, K.-J. Chao, H.-H. Cheng and C.-S. Tan, Adsorption of CO_2 onto Amine-Grafted Mesoporous Silicas, *Sep. Purif. Technol.*, 2009, **70**(1), 87–95, DOI: **10.1016/j.seppur.2009.08.016**.

50 T. Ma, E. Balanzat, J.-M. Janot and S. Balme, Nanopore Functionalized by Highly Charged Hydrogels for Osmotic Energy Harvesting, *ACS Appl. Mater. Interfaces*, 2019, **11**(13), 12578–12585, DOI: **10.1021/acsami.9b01768**.

51 F. Zhang, K. Sautter, A. M. Larsen, D. A. Findley, R. C. Davis, H. Samha and M. R. Linford, Chemical Vapor Deposition of Three Aminosilanes on Silicon Dioxide: Surface Characterization, Stability, Effects of Silane Concentration, and Cyanine Dye Adsorption, *Langmuir*, 2010, **26**(18), 14648–14654, DOI: **10.1021/la102447y**.

52 W.-M. Munief, F. Heib, F. Hempel, X. Lu, M. Schwartz, V. Pachauri, R. Hempelmann, M. Schmitt and S. Ingebrandt, Silane Deposition *via* Gas-Phase Evaporation and High-Resolution Surface Characterization of the Ultrathin Siloxane Coatings, *Langmuir*, 2018, **34**(35), 10217–10229, DOI: **10.1021/acs.langmuir.8b01044**.

53 S. Tseng, S.-C. Lin, C.-Y. Lin and J.-P. Hsu, Influences of Cone Angle and Surface Charge Density on the Ion Current Rectification Behavior of a Conical Nanopore, *J. Phys. Chem. C*, 2016, **120**(44), 25620–25627, DOI: **10.1021/acs.jpcc.6b08588**.

54 S. Qian, S. W. Joo, Y. Ai, M. A. Cheney and W. Hou, Effect of Linear Surface-Charge Non-Uniformities on the Electrokinetic Ionic-Current Rectification in Conical Nanopores, *J. Colloid Interface Sci.*, 2009, **329**(2), 376–383, DOI: **10.1016/j.jcis.2008.10.012**.

55 J. Liu, D. Wang, M. Kvetny, W. Brown, Y. Li and G. Wang, Quantification of Steady-State Ion Transport through Single Conical Nanopores and a Nonuniform Distribution of Surface Charges, *Langmuir*, 2013, **29**, 8743–8752.

56 W. Yoshida, R. P. Castro, J.-D. Jou and Y. Cohen, Multilayer Alkoxysilane Silylation of Oxide Surfaces, *Langmuir*, 2001, **17**(19), 5882–5888, DOI: **10.1021/la001780s**.

